Article

Prediction of Heat Transfer in a Hybrid Solar–Thermal–Photovoltaic Heat Exchanger Using Computational Fluid Dynamics

Sandro Guadalupe Pérez Grajales [1]**, Teresa Hernández Ortíz** [1]**, Rogelio Martinez-Oropeza** [1]**, Tabai Torres** [1]**, López-Pérez Luis Adrián** [1]**, Javier Delgado-Gonzaga** [2]**, Armando Huicochea** [1,*] **and David Juárez-Romero** [1,*]

[1] Center for Research in Engineering and Applied Sciences (CIICAp), Autonomous University of the State of Morelos, University Avenue No. 1001, Col Chamilpa, Cuernavaca C.P. 62209, Morelos, México; sandro.perez@uaem.mx (S.G.P.G.); teresahdez@yahoo.com (T.H.O.); rogelio.martinezoro@uaem.edu.mx (R.M.-O.); tabai.torres@uaem.mx (T.T.); lpladrian_84@hotmail.com (L.-P.L.A.)

[2] Institute of Renewable Energies, University Autonomous of Mexico, Xochicalco s/n Col. Azteca, Temixco C.P. 62588, Morelos, Mexico; javier.delgado@uaem.mx

[*] Correspondence: huico_chea@uaem.mx (A.H.); djuarezr7@gmail.com (D.J.-R.)

Abstract: Solar energy is one of the main renewable energy resources due to its abundance. It can be used for two purposes, thermal or photovoltaic applications. However, when the resource obtained is mixed, it is called photovoltaic thermal hybrid, where the solar panels generate electricity and are provided with a heat exchanger to absorb energy through a water flow. This is one of the techniques used by the scientific community to reduce the excess temperature generated by solar radiation in the cells, improving the electrical efficiency of photovoltaic systems and obtaining fluid with higher temperature. In this work, the thermal behavior of a heat exchanger equipped with fins in its interior to increase the thermal efficiency of the system was analyzed using CFD (Computational Fluid Dynamics). The results showed that the average fluid outlet temperature was 75.31 °C, considering an incident irradiance of 1067 W/m^2 and a fluid inlet temperature of 27 °C. The operating conditions were obtained from published experimental studies, achieving 97.7% similarity between the two. This was due to the boundary conditions of the heat flux (1067 W/m^2) impinging directly on the coupled cells and the heat exchanger in a working area of 0.22 m^2.

Keywords: heat exchanger; thermal efficiency; photovoltaic cell; PH/T

1. Introduction

This introduction presents a three-part sequence designed to give the reader a better understanding of the functionality of photovoltaic hybrid heat exchangers, based on theoretical studies on heat exchangers, photovoltaic panels, and coupled hybrid (photovoltaic–thermal) heat exchangers.

1.1. Theoretical Studies of Heat Exchangers

This work analyses the prediction of heat transformers obtained by two flat-plate solar collectors configured in series and in parallel, as well as a third system produced by the union of the two previous ones. Flat-plate solar collector systems were coupled to a water heating energy source directed to an absorption heat transformer integrated with a water purification system, maximizing efficiency. To obtain the prediction of the heat transformer, a feed-forward ANN (artificial neural network) with the standard BP (back propagation) algorithm was applied. The statistical performance criteria, i.e., RMSE (root mean square error) and R^2 (correlation), a feed-forward ANN (artificial neural network) with the standard BP (back propagation) algorithm (root mean square error) and R^2 (correlation coefficient) were applied; a supervised ANN with 5-5-1 topology (five inputs, five

neurons in the hidden layer, and one output layer) and Levenberg–Marquardt training algorithm represented the optimal model. This ANN considered the total useful irradiance, the water temperature in the heating tank, and the sampling time (second, day, and month) as input parameters; and as output parameter, the heat gained by the water in the heating tank [1]. Solar energy is currently the most affordable and abundant natural resource available as an alternative energy source in the global environment, respective of improvements in renewable energy technology [2]. The main component of solar water heater applications is the solar collector. This has been studied theoretically and experimentally in terms of optical optimization, heat loss reduction, and heat recovery improvement [3]. In related research, a detailed review of energy and exergy analyses of several typical solar energy technologies used for various heat and power generation applications was carried out [4]. The proposed technique used support vector machines for heat exchanger performance prediction during heat exchanger modeling and simulation [5]. An article reviewed the applications of ANNs (artificial neural networks) for thermal analysis of heat exchangers, as they have been widely used for thermal analysis of heat exchangers over the last two decades. The further research needs in this field are discussed according to the published research on heat exchanger thermal analysis, by classifying them into four main groups: (I) heat exchanger modelling, (II) heat exchanger parameter estimation, (III) estimation of phase change characteristics in heat exchangers, and (IV) heat exchanger control. In conclusion, ANNs are gaining popularity as a tool that can be successfully used for thermal analysis of heat exchangers with acceptable accuracy [6]. An article discussed the types of solar collectors to facilitate the systematic understanding of solar thermal technology, in order to attract beginners in the field of solar thermal conversion technology [7]. In that research, the configuration of a plate heat exchanger was analyzed by a two-dimensional numerical model using the effective heat capacity method [8]. In that work, MATLAB software was used to theoretically model a flat-plate solar collector using nanofluids as a heat transport medium [9]. A stainless-steel flat-plate solar collector (S-S FPSC) was studied using numerical simulation models as a basis for optimization research, where the flow resistance of the microchannels was analyzed to define their structural parameters [10]. A study was carried out in the city of Al-Samawa, Iraq, in which an active flat-plate solar collector (FPSC) with an internal absorber tube receiver was fabricated and tested, simulated, and validated in TRNSYS [11]. In that study, a model was developed to calculate the heat losses of the FPSC, analyzing the integral impact of altitude change on the heat loss performance of the FPSC; the accuracy of the model was verified using experimental test data [12]. In another study, a numerical simulation of a typical flat-plate solar collector was performed, where the governing differential equations were solved numerically using the finite difference method and the transient problem was formulated using an implicit scheme able to provide a stable solution for any mesh size [13]. In further work, numerical simulation models for both large flat-plate solar collectors (LSFPSCs) and conventional parallel FPSCs were studied. Subsequently, the effects of environmental and operational parameters on the thermal performance of the two types of collectors were investigated by analyzing their applicability with respect to available operating times, useful energy, and heat loss [14]. That work determined the most used methods to improve FPSC efficiencies through the use of CFD [15]. Solid Work and CFD software were used to analyze the meshing and fluid flow with aluminum and copper materials to see which was more efficient [16]. The performance of a flat-plate heat exchanger was studied by simulation using finite volume methods describing the absorber plate temperature field and flow conditions; the results of the investigation helped to design and optimize the heat pipe flat-plate heat exchanger [17]. A three-dimensional CFD transient model was used in Shiraz, Iran, to investigate a flat-plate heat exchanger integrated with a PCM layer [18]. The operation of the flat plate-heat exchanger was modeled using three different fluid flow rates of water (1, 1.6, and 2 L/min), employing an artificial neural network (ANN). The results obtained confirmed that the method was accurate with all three flow rates of the working fluid (water) [19]. Another paper proposed a thermodynamic model based on

simplified semi-empirical correlations. The model was used to evaluate the performance of the latent heat storage technique in a flat-plate heat exchanger (FPSC) with integrated phase-change material (PCM) [20].

1.2. Theoretical Studies on Photovoltaic Panels

Talking about energy and ways of obtaining this resource without harming the environment has become a major topic. One type of system that harnesses solar energy is the flat-plate heat exchanger or flat-plate solar collector [15]. Therefore, various methodologies have been employed to improve their thermal efficiency and performance by harnessing solar energy, including the coating and thickness of the glass envelope, as well as the transmittance and emissivity of the glass envelope [21]. There have also been investigations where the steady-state thermal performance of a flat-plate heat exchanger was studied using the finite volume method [22]. Another way to improve efficiency is with coatings, as shown in the article "Simulation study on the efficiency of thermochromic absorber coatings for solar thermal flat-plate collectors" [23]. A comparison of simulations was carried out to evaluate the efficiency and performance of commercially available absorber coatings for flat-plate solar heat exchangers, obtaining an increase in auxiliary energy demand of 6% with black chrome, 7% with thermochromic chrome, and 21% with solar paints, compared with PVD coatings [24]. It is important to mention the new technologies applied to this type of systems, such as the use of nanofluids, as observed in the research "Finite Element Simulation of Forced Convection in a Flat Plate Solar Exchanger: Influence of Nanofluid with Dual Nanoparticles" [25]. Applications of this type of solar heat exchanger can be observed in the research "Numerical simulation and parametric study of different types of solar cooling systems under Mediterranean climatic conditions" [26] and also, the "Performance evaluation and theoretical simulation of an adsorption refrigeration system driven by a flat plate solar collector" [27]. The second type of solar collector is an evacuated tube heat exchanger device used to capture solar energy, applicable in both domestic and industrial environments. Computational fluid dynamics (CFD)-based studies exploring the use of nanofluids and phase-change materials to improve the efficiency of ETSCs have been discussed [28]. This type of collector can also be coupled to other systems, as reported in the investigation of "Theoretical model of an integrated evacuated tube solar collector with phase change material", where the aim was to theoretically model a solar hot water system consisting of a set of ETHPSCs (evacuated tube solar collectors) connected to a common collector filled with phase-change material and acting as a LHTES (latent heat thermal energy storage) reservoir [29]. The last in the category of solar collectors are tube solar heat exchangers, which were introduced to overcome the limitations of the first two groups of solar collectors by exploiting the advantages of heat pipes and ETSC technologies. Low thermal resistance, high heat removal from the absorber surface, and low hydraulic resistance are some of the advantages of this type of collector [30].

1.3. Theoretical Studies on Hybrid (Thermal–Photovoltaic) Heat Exchangers

After reviewing the theoretical literature, no work was found on a hybrid photovoltaic thermal exchanger simulated with the characteristics of combining photovoltaic cells with heat exchangers or solar thermal collectors to allow cogeneration of electricity and hot water for different processes [31]. The energy captured from the sun comes from a clean energy source and reaches thermal levels ranging from 60 to 280 °C and up to 400 °C via equipment for power generation systems [32]. Majdi Hazami et al. determined the theoretical performance of photovoltaic cells through simulations in Tunisian North Africa [33]. Hybrid heat exchangers coated with silver with low emissivity were fabricated for simulation and experimentation [34]. Large deviations (up to 20 °C) of the base plate temperature in the correlations compared with the experimental results were observed in the modeling, probably due to the geometrical characteristics of the heat exchanger [35]. The numerical performance of a solar-assisted heat pump coupled to a photovoltaic air heater was studied, demonstrating the feasibility of the project [36]. The modeling of a

low-concentration photovoltaic system was studied using various analytical correlations and CFD simulations to monitor module temperature and improve analyze electrical efficiency [37]. Some researchers have identified environmental design factors, such as mass flow rate and inlet water temperature [38]. PV/T modules combine efficiencies from 40 to 87% and can be applied in ground, wall, or rooftop installations in urban and rural areas to supply energy [39]. Temperature rises and efficiency have been analyzed using active and passive cooling methods. In these processes, water is typically used as the cooling medium [40]. A parameter investigation was carried out based on the height, number of, and distance between fins. The effect of solar irradiance on PV module performance was evaluated by CFD, ANSYS FLUENT using 3D Navier–Stokes energy equations for numerical calculations [41]. In related work, a solar heating and cooling (SHC) system including thermal/photovoltaic (PV/T) heat exchangers was considered, implementing a polygeneration system. The performance of the system was analyzed from an energy and economic point of view using a zero-dimensional transient simulation model developed with TRNSYS, and the results were compared with those reported in the literature [42]. In a study carried out in Changping, Beijing, China, the performance of a low-concentration photovoltaic/thermal module (LC-PV/T) was evaluated numerically using MATLAB software and experimentally by analyzing its performance under different operating conditions (fixed flow rate and output temperature) [43]. In that study, a low-concentration photovoltaic/thermal triple generation system for heating, cooling, and electricity was proposed. To demonstrate its feasibility, the performance of the system was dynamically simulated using the Transient Systems Simulation Program (TRNSYS) software [44]. Parametric studies and annual transient simulations of hybrid photovoltaic-thermal (PV/T) solar systems have been modeled by Simulink/MATLAB [45]. Thermodynamic modeling of the thermal and electrical performance of a hybrid heat exchanger (PV/T) was carried out and used for the design of a new absorber (double oscillating absorber). The results of the hybrid PV technology were compared with those of normal PV technology (without cooling systems) by a simulation analysis of the model based on theoretical data, using MATLAB [46]. In other work, an investigation was carried out on the impact of adapting to a non-uniform PV temperature along the receiver. For this purpose, a 2D heat transfer model of a (PV/T) system was created [47]. Further study analyzed the development of a theoretical dynamic model to predict the long-term performance of a (CPV/T) photovoltaic/thermal parabolic trough system. The results showed that the system's exergy performance was mainly influenced by the trough and the electrical efficiency of the PV module [48]. A thermomagnetic finite element model (FEM) of the CPV/T in 2D and 3D has been developed, capable of calculating the heat transfer that occurs due to the cooling fluid flow, obtaining a significant influence on the performance when operating in climatic zones with very different temperature ranges throughout the year [49]. A parabolic trough heat exchanger was designed and simulated to simultaneously generate electricity and high-temperature thermal energy [50]. A mathematical model was presented using the Microsoft Excel "Goal-Seek" data tool to describe the performance of a concentrated photovoltaic system where the thermal energy rejected by the photovoltaic cell was used to distill salt water [51]. Using COMSOL and SolidWorks, a combined thermal and optical three-dimensional analysis of an asymmetric compound parabolic collector (ACPC) with a hybrid photovoltaic/thermal (PV/T) receiver was presented. Initially, the incident angle modifier was calculated and numerical models verified against each other by simulation tools were used in the thermal analysis part and validated by experimental results extracted from the literature on the examined collector [52]. For a new type of trough photovoltaic/thermal composite heat exchanger with change suspension, a three-dimensional physical model was proposed and studied numerically, thus evaluating the dynamic performance of the hybrid photovoltaic/thermal collector [53]. Numerical calculations were performed for two climatic conditions in India, first in January (winter) and then in June (summer), taking the thermal energy balance equations for N partially covered parabolic trough concentrators (N-PV/T-CPCs) connected in sequence [54]. Those authors numerically developed two convergent channel

configurations of photovoltaic–thermal (PV-T) systems, i.e., inlet and outlet on different sides (case 1) and inlet in the middle and outlets on the sides (case 2). They achieved up to 500 W of additional power per unit area of PV module by exchanging one PV system for its proposed counterpart, thereby reducing the levelized cost of energy in the PV system compared with the stand-alone system. These stand-alone PV systems showed a net CO_2 mitigation of 10% compared to conventional PV systems [55]. The authors investigated the efficiency of a concentrating photovoltaic/thermal (CPV/T) device. The simulation considered multi-tube PV/T systems, with and without the inclusion of twisted ribbons, using H_2O as the test fluid. The influence of the concentration ratio was evaluated by varying the incident irradiances equivalent to one, two, or three suns. The results showed that using the CPV/T system under three suns with the optimal design would to a reduction of approximately 5541 kg of carbon emissions over 10 years [56]. These authors performed a numerical analysis of a photovoltaic system aimed at improving efficiency by incorporating an absorber consisting of finned tubes, through which water and air circulated as working fluids. With this approach, a thermal efficiency of 54% was achieved [57]. Similarly, others investigated the efficiency of a photovoltaic-thermal (PV/T) system using a collective cooling method with internal plate thermal fins, employing nanofluids (Al_2O_3, TiO_2, and CuO) as coolants. Their results indicated that the Al_2O_3–water nanofluid with 0.2% nanoparticles achieved the highest thermal efficiency, with an average of 49.59% [58]. To conclude this introduction, the work was simulated in Ansys Fluent to observe the behavior of the theoretical parameters statically and assess their capacity to produce thermal and electrical energy, according to the experimental data taken from a prototype designed, built, and evaluated. These results are important to verify the technical capability of the fins added to the interior that were used to improve the heat transfer in combination with the mass flow, and to thus indicate the excellent thermal–electrical capabilities and future commercial performance of this prototype. There is currently no commercial solar heat exchanger with integrated fins inside.

2. Description of the Heat Exchanger and Governing Equations

2.1. Heat Exchanger and Governing Equations

To model the hybrid solar system, we used the principle of energy conservation for each component of the system. We present the equations used in the experimental work as follows: thermal efficiency (Equation (1)), working temperature (Equation (2)), working power (Equation (3)), photovoltaic efficiency (Equation (4)) and total photovoltaic–thermal efficiency (Equation (5)), which are detailed in Table 1. Equations (1) and (2) are based on the effect of the temperature caused by the incident solar radiation on the photovoltaic cells. Equations (1) and (2) are based on the effect of the temperature caused by the incident solar radiation on the photovoltaic cells. The working temperature (T_t) reached by a photovoltaic panel obeys a linear relationship given by the expression in Table 1, in which it is stated that the said temperature will depend on the ambient temperature, radiation, and the coefficient of variation (this will depend on the wind speed if it is 0.2 to 0.4 °C·cm²/mW) at which it is operating for the cooling of the cells. In conclusion, (K*R) represents the temperature rise of the cells above the maximum ambient temperature and therefore affects the performance.

Table 1. Representation of the equations used in the experimental work.

Equations	Calculation	Equation Number	References
$\eta = \frac{\dot{m} \cdot C_p (T_{out} - T_{in})}{G \cdot A}$	Efficiency thermal substituting Qu for its value, in the Bliss equation. We have:	(1)	[59]
$T_t = T_a + K \cdot R$	Works temperature	(2)	[60]
$P_t = P_p - (P_p \cdot \delta \cdot \Delta T)$	Working power	(3)	[60]
$\eta_{Pv} = \frac{I_{max} \cdot V_{max}}{G \cdot A}$	Photovoltaic efficiency	(4)	[61]
$\eta_{Pv/Th} = \frac{I_{max} \cdot V_{max}}{G \cdot A} + \frac{\dot{m} \cdot C_p (T_{out} - T_{in})}{G \cdot A}$	Total photovoltaic–thermal efficiency	(5)	[61]

To calculate the output power at the working temperature (P_t) reached by a photovoltaic panel, the first step is to calculate the working temperature and then determine the increase in temperature with respect to the test temperature (25 °C), which is resolved as Δt: temperature increase over 25 °C ($T_t - 25$ °C). The peak power is given by the manufacturer at room temperature, as well as the degradation coefficient.

2.2. Photovoltaic Thermal Model

This model is solved by the equations for each of these components, based on the analysis of the energy balance, photoelectric conversion, thermal conductivity, convection, and radiation. It includes the panel absorbance (α_s), solar radiation (G), panel area (A_s), ambient temperature (T_a), rad, convec, and conduct heat transfer coefficients ($h_{rad}, h_{convec}, h_{conduct}$), solar cell temperature (S), and plate temperature (T_p). Figure 1 shows the PV thermal model, illustrating the heat transfer processes (conduction, convection, and radiation) that occur both inside and outside the hybrid solar equipment to produce the desired results (heat and electricity). The process is divided into three components: the PV panel, the solar cells, and the fluid (water). Here, the important part of the study is the heat flow of the maximum experimental radiation incident on the PV cells, which is used to theoretically evaluate the heat transfer as represented in Equations ((6)–(8)). The thermal energy balance for solar power generation is based on photoelectric conversion, thermal conductivity, convection, and radiation. It includes panel absorbance, solar radiation, panel surface area, ambient temperature, heat transfer coefficients, and solar cell and plate temperatures [62].
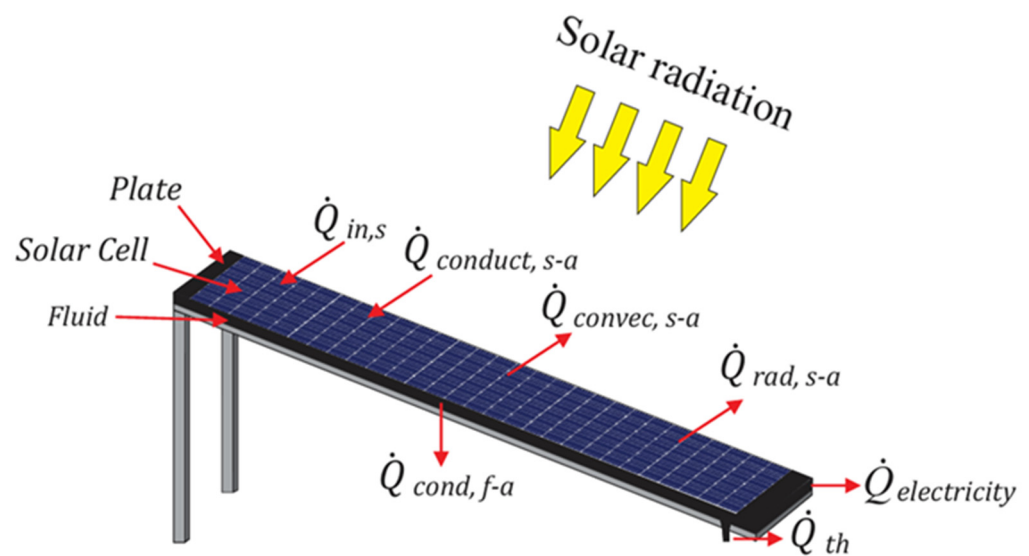

Figure 1. Model PV/T.

Energy balance for solar cells:

$$\dot{Q}_{be,S} = \dot{Q}_{in,s} - \dot{Q}_{rad,s-a} - \dot{Q}_{convec,s-a} - \dot{Q}_{conduct,s-a} - \dot{Q}_{electricity} \tag{6}$$

$$\dot{Q}_{be.S} = \alpha_s \cdot A_s \cdot G - A_s \cdot \hbar_{rad} \cdot (T_s - T_a) - A_s \cdot \hbar_{conduct} \cdot (T_s - T_p) - \eta_s \cdot \alpha_s \cdot G \cdot A_s$$

Energy balance for the absorber plate:

$$\dot{Q}_{be,P} = \dot{Q}_{conduct,\ s-p} - \dot{Q}_{conduct,p-a} - \dot{Q}_{conduct,P-f} \tag{7}$$

$$\dot{Q}_{be,P} = A_s \cdot \hbar_{conduct} \cdot (T_s - T_p) - A_s \cdot \hbar_{conduct} \cdot (T_p - T_a) - q_f$$

Energy balance for the fluid:

$$\dot{Q}_{be,f} = \dot{Q}_{conduct,f-a} + \dot{Q}_{th} \tag{8}$$

$$\dot{Q}_{be,f} = A_f \cdot \hbar_{conduct} \cdot (T_f - T_a) - \dot{m} \cdot C_P \cdot (T_{fo} - T_{fi})$$

3. Numerical Model

The aim of this study was to calculate, by means of 3D numerical simulation, the amount of heat absorbed when installing a heat exchanger under a solar photovoltaic cell. The case study presented refers to a hybrid photovoltaic system consisting of a set of photovoltaic cells installed on a heat exchanger, which is an aluminum channel 1670 mm long and 290 mm wide, equipped inside with 12 pairs of fins with an inclination of 60 °C with respect to the direction of flow, and an intermediate bulkhead, through which a fluid (water) passes to extract the heat produced by the solar cell and obtain hot water at the outlet. It should be noted that the solar cells were installed centered on the top wall of the heat exchanger by means of an absorber plate and covered an area of 0.228 m² (1.64 m long and 0.139 m wide) to increase the heat exchange; the model is shown in Figure 2. Studies have shown a favourable impact on the photovoltaic electrical efficiency by decreasing the temperature of the solar panel [63]. The characteristics of the heat exchanger are shown in Figure 3.
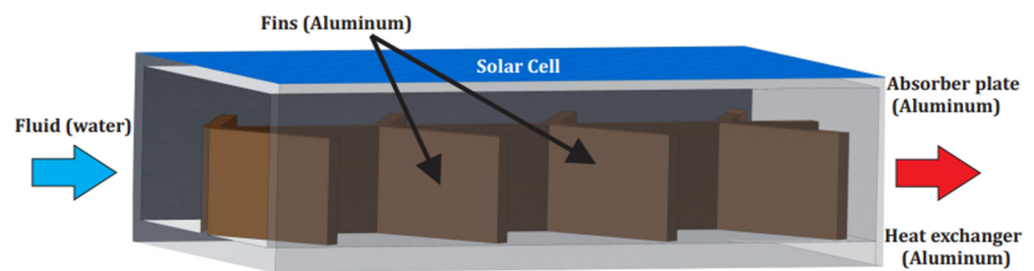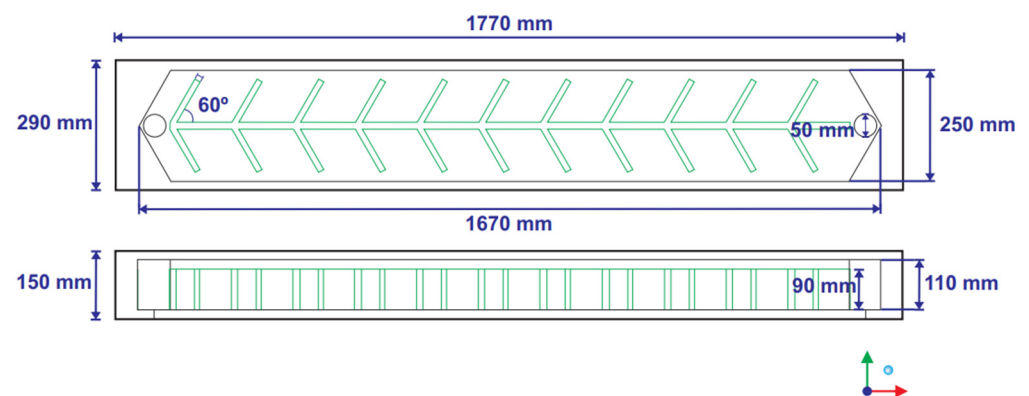

Figure 2. Model of hybrid photovoltaic system.

Figure 3. Model of Heat Exchanger.

3.1. Geometry and Discretization

The evaluated numerical model included two computational domains: (1) the solid (aluminum), consisting of the finned heat exchanger and the solar PV cell, and (2) the fluid domain, representing the water flowing inside the cell. Both domains were generated using ICEM CFD, as illustrated in Figure 4. An unstructured mesh was applied to discretize these domains, with specific refinement levels at the fin walls to enhance accuracy in regions critical for heat exchange.
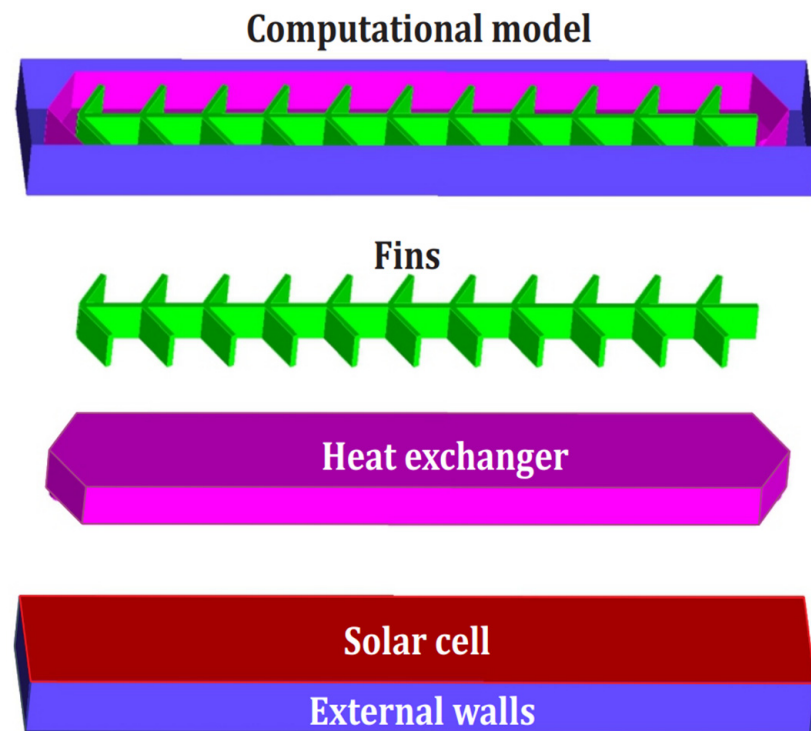
Computational model

Fins

Heat exchanger

Solar cell

External walls

Figure 4. Computational model.

The determination of the best mesh was based on the computation time used, by calculating the relative error percentage, as shown in Table 2, considering the average temperature at the heat exchanger outlet as the measurement variable. In this study, in the search for optimization of the computation time, mesh 2 was used, which obtained a relative error of 0.87%. The mesh refinement near the fin wall had a minimum cell size of 4 mm, as shown in Figure 5. In Figure 6, the structure of the work is represented by a flow chart.
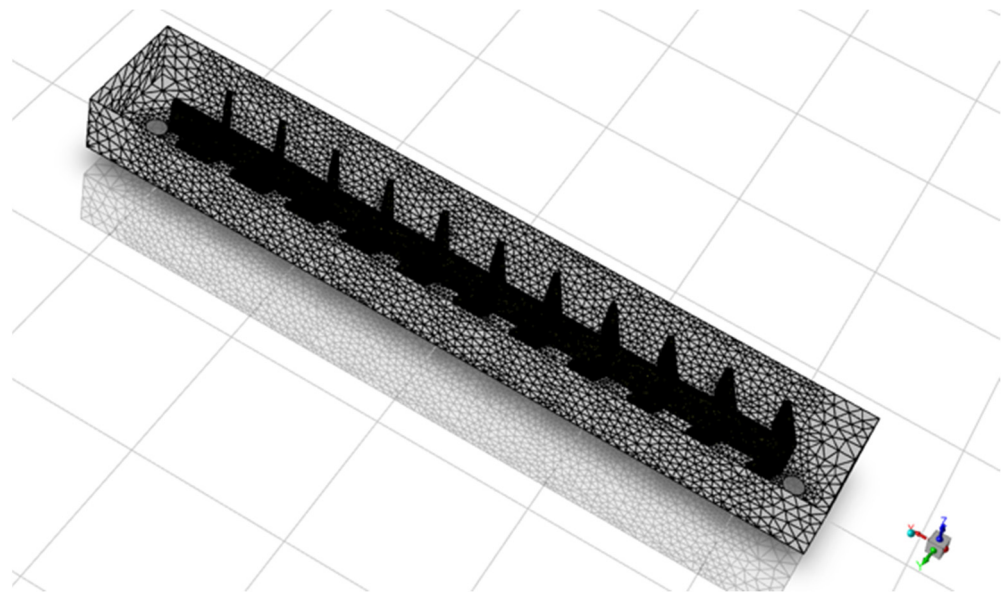
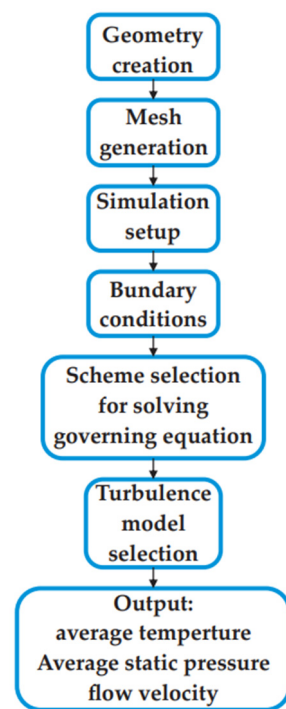**Figure 5.** Discretization of the computational model.

Figure 6. Flow Chart.

Table 2. Mesh independence.

Mesh	Elements	Mesh Type	Average Temperature [°C]	%ε_r
Mesh 1	2,941,907	Tetrahedral	74.66	
Mesh 2	**1,860,633**	**Tetrahedral**	**75.31**	**0.87%**
Mesh 3	1,452,591	Tetrahedral	75.40	0.98%
Mesh 4	1,332,107	Tetrahedral	75.48	1.09%
Mesh 5	1,153,646	Tetrahedral	75.86	1.60%

3.2. Governing Equations on the Numerical Model

The model of the solar thermal hybrid system evaluated in this study considered the stationary heat transfer in solids without heat generation and the stationary heat transfer in the fluid using the energy conservation equation. Considering for the solid the thermal conductivity k in Equation (9) and for the fluid, the rate of convective heat transfer $\rho C_p u \cdot \nabla T$ in Equation (10), where u is the fluid velocity. In the solar cell, the heat flux due to solar irradiation is defined by G, being incident in the form of a vector normal to the surface n, as seen in Equation (11).

$$\nabla \cdot (k \nabla T) = 0 \tag{9}$$

$$\rho C_p u \cdot \nabla T = \nabla \cdot (k \nabla T) \tag{10}$$

$$-n \cdot (-k \nabla T) = G \tag{11}$$

The model included convection with the atmosphere, calculated from the heat transfer coefficient h and the temperature difference between the atmosphere and the solar panel, as shown in Equation (12). Radiative heat transfer was also included in the model:

$$-n \cdot (-k \nabla T) = h \cdot (T_{amb} - T) \tag{12}$$

The solution of the flow involved solving the continuity equation, the equations of motion, and the turbulence model. Due to the low-velocity flow, low Reynolds number, and compressibility, the standard k-ω turbulence model was chosen, an empirical model based on model transport equations for the turbulence kinetic energy k and the specific dissipation rate ω, which can also be thought of as the ratio of ε to k. The turbulence kinetic energy and the specific dissipation rate were obtained from Equations (13) and (14):

$$\frac{\partial}{\partial t}(\rho k) + \frac{\partial}{\partial x_i}(\rho k u_i) = \frac{\partial}{\partial x_j}\left(\Gamma_k \frac{\partial k}{\partial x_j}\right) + G_k - Y_k + S_k \tag{13}$$

$$\frac{\partial}{\partial t}(\rho \omega) + \frac{\partial}{\partial x_i}(\rho \omega u_i) = \frac{\partial}{\partial x_j}\left(\Gamma_\omega \frac{\partial \omega}{\partial x_j}\right) + G_\omega - Y_\omega + S_\omega \tag{14}$$

where G_k represents the generation of turbulence kinetic energy due to the mean velocity gradients. G_ω represents the generation of ω, Γ_k and Γ_ω represent the effective diffusivity of k and ω, respectively. Y_k and Y_ω represent the dissipation of k and ω due to turbulence [64].

3.3. Boundary Conditions

The numerical study was based on incompressible URANS simulations in 3D to solve the aforementioned governing equations and obtain the temperature distribution along a mean plane inside and at the heat exchanger outlet. The calculations were performed stationary by setting up a SIMPLE algorithm for the pressure–velocity coupling, and a second-order scheme was used for discretizing the momentum and energy equations.

The solutions converged, satisfying predefined criteria (ranging from 1×10^{-6} for continuity and energy) for the continuity equation, momentum equation, and energy equation, respectively. A direct heat flux of 1067 W/m^2 was applied in the cell based on experimental data obtained from the literature [65], considering an external temperature of 26.5 °C. A coupled wall with a no-slip condition was configured on both the inner walls and the fins, while a convective heat transfer coefficient was set for the outer walls. A uniform mass flow of 0.01 Kg/s was established at the fluid inlet, with a temperature of 27 °C and a pressure of 1 atm. For the outlet, a pressure outlet was used to ensure mass continuity at 1 atm. The flow inside the exchanger was solved using standard $k - \omega$ turbulence model, and five measurement points were set up at the outlet to monitor the flow temperature. The boundary conditions are listed in Table 3. The properties of the materials used are shown in Table 4, and the measurement points at the outlet are shown in Figure 7. These monitors were used to calculate the average temperature at the outlet of the exchanger.

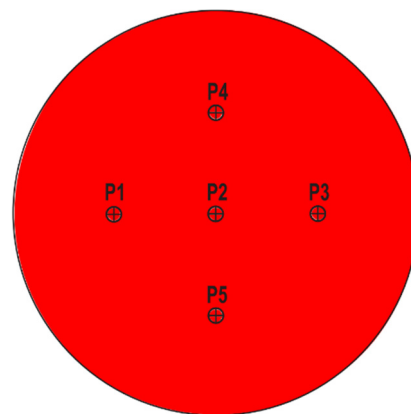**Table 3.** Boundary conditions in the model.

Name	Boundary
Solar cell	Heat flux
External walls	Convection
Inlet	Mass flow inlet
Outlet	Pressure outlet
Fins	Wall with no-slip condition
Heat exchanger	Coupled wall

Table 4. Properties of the materials.

Material	Property	Value
Solar cell	ρ	2329 Kg/m^3
	k	130 W/m·k
	Cp	700 J/kg·k
	ε	0.60

Table 4. *Cont.*

Material	Property	Value
Aluminum	ρ	2699 Kg/m^3
	k	209 W/m·k
	Cp	102 J/kg·k
Water	ρ	997 Kg/m^3
	k	0.611 W/m·k
	Cp	4.184 kJ/kg·k
	μ	902×10^{-6} kg/m·s

Figure 7. Temperature monitors at the outlet of the heat exchanger.

4. Results and Discussion

4.1. Static Analysis of Heat Transfer in a Hybrid Photovoltaic Heat Exchanger

A three-dimensional model was simulated in Ansys Fluent software, to analyze cooling of the photovoltaic cells by water flow. The process consisted of dissipating heat from the cells, which facilitated better absorption of heat from the heat transfer fluid. The model setup included the Navier–Stokes energy, continuity, and momentum equations, which were subsequently solved. The radiation problem was solved through the boundary conditions (heat flux of 1067 W/m^2), in which the main contribution of the design is the fins. Although it is known that in Spain, finned tube heat exchangers (referring to non-solar heat pumps) are beginning to be used, we implemented it in photovoltaic solar exchangers to obtain a better performance in the cooling of the cells and an improvement in the electrical performance, as well as obtaining a thermal performance as demonstrated in the experimental work referenced in the previous paragraph.

Figure 8a shows the temperature contour of the lateral plane where the solar photovoltaic heat exchanger reached 87.1 °C, which was absorbed by the heat transfer fluid, reducing the cell temperature and providing the cooling fluid with approximately 75.31 °C. The middle lateral plane facilitates the observation of the thermal drag experienced by the water as it entered the exchanger and directly impacted the surface of the solar cell. This interaction resulted in a temperature change from 27 °C (inlet temperature) to 56.7 °C by the third row of fins. This region exhibited the highest thermal exchange due to the turbulence generated by the change in flow direction and the interaction of the flow with the fin walls. Subsequently, the flow continued to increase in temperature until it reached the outlet, where a significant temperature change occurred as the flow direction was altered once again.

Figure 8b shows that during the simulation process, the temperature of the midplane and the heat distribution through the flow inside the equipment and through the fins gradually increased as a consequence of the solar radiation of 1067 W/m^2 that directly reached the PV cells and the housing of the equipment. This plane allows us to visualize the

impact of the fins on the water flow and, consequently, on the thermal exchange. Since the fins are attached to the casing, the flow is forced to recirculate within the internal sections, resulting in a gradual temperature increase at the internal vertices of each fin as the water progresses toward the outlet.
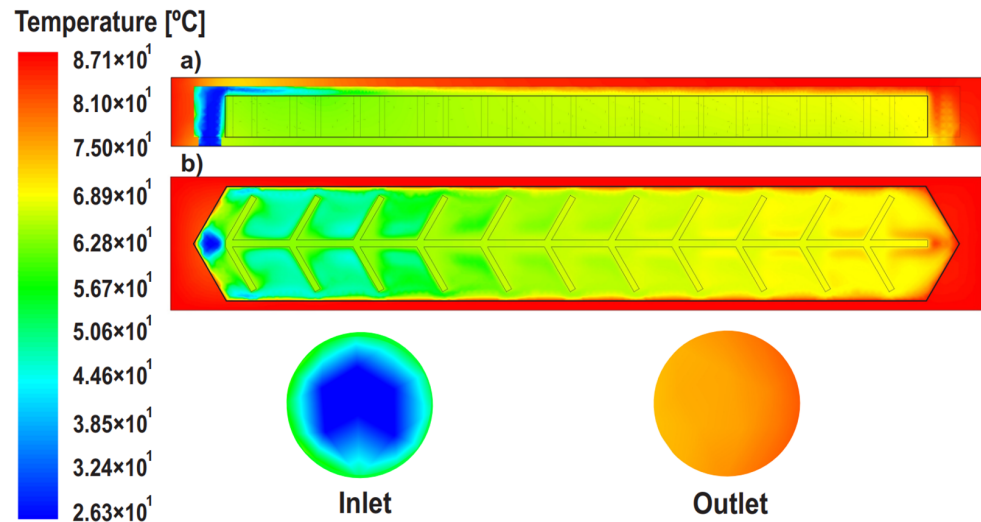

Figure 8. (**a**,**b**) Temperature contour of the lateral plane and midplane.

In Figure 9, we can see that during the simulation process, there was a small pressure drop due to the turbulence that existed when the fluid collided with the walls of the equipment and the velocity of the fluid as it travelled through the heat exchanger.
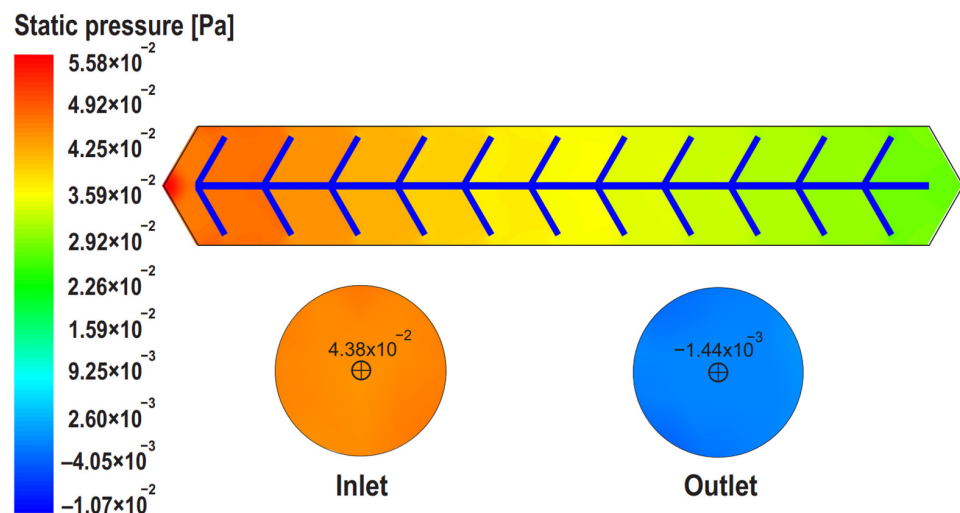

Figure 9. Static pressure of the fluid in the heat exchanger.

In Figure 10, we see the velocity in a mid-plane contour in the simulation at 0.00544 m/s. A heat exchange with the photovoltaic cells was generated; due to the incidence of the solar radiation of 1067 W/m², they reached 87.1 °C in temperature. When the process finished, the fluid had taken on the greater thermal part produced by the phenomenon.

Figure 11 shows how the liquid temperature was distributed at the exchanger outlet, for which the temperature of the five monitors is shown. The stability of the temperature can be observed at approximately 150 iterations, where the highest temperature was 75.31 °C. It should be noted that the measurement points are numbered from 1 to 5, as shown in Figure 8, with P4 being the first monitoring point after the last fin and P5 being the last monitoring point near the outlet of the exchanger. A significant temperature change was

observed at P5 because the flow at that point experienced greater recirculation, resulting in enhanced thermal exchange. Consequently, an average of the measurement points was calculated to determine the outlet temperature of the flow.
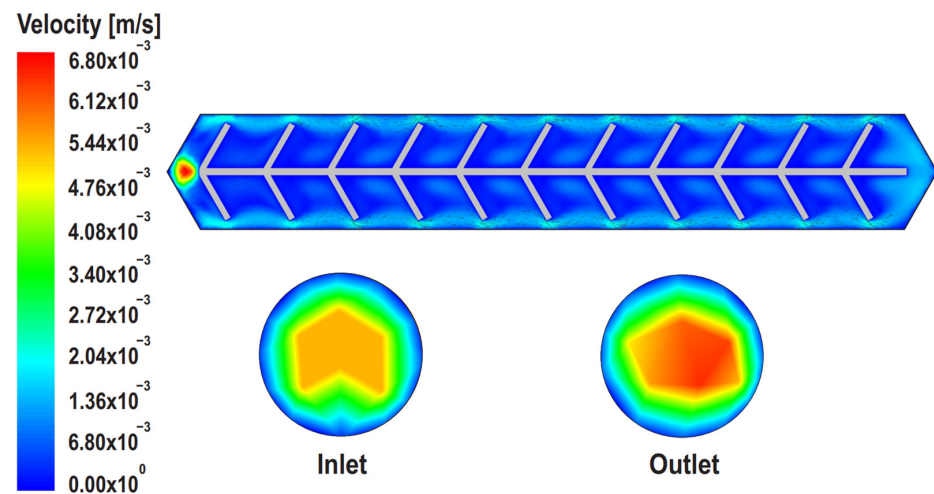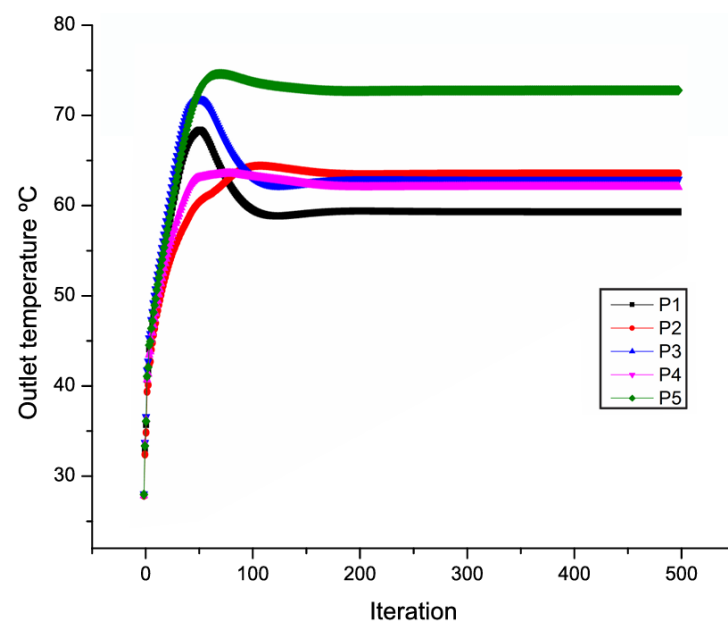

Figure 10. Velocity contours in the midplane.

Figure 11. Temperature at the outlet of the heat exchanger.

4.2. Final Remarks

It was possible to prove that the experimental results were due to the fact that the 12 fins added in the interior imparted excellent performance in improving the heat transfer in combination with the mass flow; so, the theoretical thermal performance obtained a relative error of 2.3%, and the literature mentions that it should be less than 10%. All this was due to the reduced geometrical characteristics with a mass flow of 0.01 kg. To complete these observations, we conclude that the 97.7% similarity refers to the thermal results of the experiment and simulation. We do not focus on the electrical performance, as it is well known that as the cell temperature decreases, its efficiency improves. A lot of the published literature affirms this, as can be seen in the introduction provided.

5. Conclusions

The numerical analysis presented in this manuscript aims to improve both photovoltaic and thermal cogeneration, specifically by achieving higher water temperatures at the

exchanger outlet. For this purpose, the inlet mass flow rate of 0.01 kg/s was kept constant. The novelty of this work is the incorporation of fins to improve heat transfer efficiency by increasing the contact surface between the fluid and solid at higher temperatures, as well as improving turbulence within the heat exchanger, as we did not find any work on solar photovoltaic hybrid heat exchangers in the literature, as discussed in our introduction. Furthermore, the results obtained from the proposed model were compared with the experimental data reported in the literature, referenced in Section 3.3, showing a similarity of 97.7%, especially for the thermal measurements. The data obtained in this work from the simulations in relation to the previously published experimental data were as follows. The cell temperature decreased by approximately 11.79 °C due to heat absorption by the cooling fluid, resulting in a fluid temperature of 75.31 °C at the end of the experiment. The simulation was performed using a standard k-ω turbulence model. These results were analyzed in terms of the boundary conditions at which the heat flux (1067 W/m^2) impinged on the radiative photovoltaic heat exchanger.

Author Contributions: Conceptualization, R.M.-O. and D.J.-R.; Methodology, S.G.P.G., R.M.-O. and T.T.; Validation, L.-P.L.A., J.D.-G., A.H. and D.J.-R.; Formal analysis, T.T., L.-P.L.A., A.H. and D.J.-R.; Investigation, S.G.P.G. and T.H.O.; Data curation, J.D.-G.; Writing—original draft, S.G.P.G., T.H.O. and R.M.-O.; Writing—review & editing, S.G.P.G. and A.H.; Visualization, D.J.-R.; Supervision, A.H. and D.J.-R. All authors have read and agreed to the published version of the manuscript.

Data Availability Statement: The data presented in this study are available on request from the corresponding author.

Conflicts of Interest: The authors declare that there are no conflicts of interest.

Abbreviations

Symbol	Description	Units
A	Total useful irradiance of the panel surface	kW/m^2
As	PV panel area	m^2
Cp	Heat capacity	J/(kg °C)
Connect	Convection	--------
Conduct	Conduction	--------
Electricity	Electricity output	--------
h	Heat transfer coefficient	W/m^2 °C
I	Current	A
K	Coefficient of variation	°C. cm^2/mW
ṁ	Mass flow	kg/s
P	Output power at a working temperature	W
P*p*	Panel peak power (25 °C).	--------
P	Plate	--------
PV/T	Photovoltaic thermal system	--------
Q	Energy	W
Q̇	Heat flow rate of power	kW
Qu	Amount of useful energy extracted per area	kW/m^2
rad	Radiance	
R	Solar radiation [varies between 80 and 100 mW/cm^2]	mW/cm^2
S	Solar cell	--------
G	Incident solar radiation absorbed by area	W/m^2
T	Temperature	°C
V	Voltage	V

Subscripts	Description
a	Environment
be	Energy balance
electricity	Electricity
Pv, *in*	Photovoltaic panel input
f	Fluid
in	Inlet
max	Maximum
out	Outlet
P_{IN}	Input power
SPs	Solar panels
s-a	Output of the photovoltaic panel to the environment
s	Solar cell
t	Work
wall	Wall
w	Water
Greek letters	**Description**
α	Vessel or panel absorbance (dimensionless)
α_s	PV panel absorptivity
Δ	Delta
Δt	Temperature increases above 25 °C ($T_t - 25$°C)
Δ	Degradation coefficient
η	Efficiency (dimensionless)
Λ	Thermal conductivity [W/(m°C)]
T	Transmittance of glass cover [dimensionless]

References

1. Hernández, T.; Pérez, S.G.; Flores, O.; Hernández, J.A.; Juárez-Romero, D.; Álvarez, A.; Galaviz-Rodriguez, J.V. Heat transfer prediction on flat solar collectors for the water purification system integrated into an absorption heat transformer. In Proceedings of the EDS Conference on Desalination for the Environment: Clean Water and Energy, Rome, Italy, 22–26 May 2016; Volume 22, p. 26.
2. Awasthi, A.; Shukla, A.K.; SR, M.M.; Dondariya, C.; Shukla, K.N.; Porwal, D.; Richhariya, G. Review on sun tracking technology in solar PV system. *Energy Rep.* **2020**, *6*, 392–405. [CrossRef]
3. Jamar, A.M.Z.A.A.; Majid, Z.A.A.; Azmi, W.H.; Norhafana, M.; Razak, A.A. A review of water heating system for solar energy applications. *Int. Commun. Heat Mass Transf.* **2016**, *76*, 178–187. [CrossRef]
4. Sansaniwal, S.K.; Sharma, V.; Mathur, J. Energy and exergy analyses of various typical solar energy applications: A comprehensive review. *Renew. Sustain. Energy Rev.* **2018**, *82*, 1576–1601. [CrossRef]
5. Muthukrishnan, S.; Krishnaswamy, H.; Thanikodi, S.; Sundaresan, D.; Venkatraman, V. Support vector machine for modelling and simulation of heat exchangers. *Therm. Sci.* **2020**, *24 Pt B*, 499–503. [CrossRef]
6. Mohanraj, M.; Jayaraj, S.; Muraleedharan, C. Applications of artificial neural networks for thermal analysis of heat exchangers–a review. *Int. J. Therm. Sci.* **2015**, *90*, 150–172. [CrossRef]
7. Suman, S.; Khan, M.K.; Pathak, M. Performance enhancement of solar collectors—A review. *Renew. Sustain. Energy Rev.* **2015**, *49*, 192–210. [CrossRef]
8. Nekoonam, S.; Ghasempour, R. Optimization of a solar cascaded phase change slab-plate heat exchanger thermal storage system. *J. Energy Storage* **2021**, *34*, 102005. [CrossRef]
9. Geovo, L.; Dal Ri, G.; Kumar, R.; Verma, S.K.; Roberts, J.J.; Mendiburu, A.Z. Theoretical model for flat plate solar collectors operating with nanofluids: Case study for Porto Alegre, Brazil. *Energy* **2023**, *263*, 125698. [CrossRef]
10. He, Y.; Yu, H.; Duan, G.; Wang, Y.; Yang, Q.; Feng, L.; Zhang, J. Thermal performance and experimental analysis of stainless-steel flat plate solar collector with full-flow channels. *Heliyon* **2024**, *10*, e28255. [CrossRef]
11. Al-Manea, A.; Al-Rbaihat, R.; Kadhim, H.T.; Alahmer, A.; Yusaf, T.; Egab, K. Experimental and numerical study to develop TRANSYS model for an active flat plate solar collector with an internally serpentine tube receiver. *Int. J. Thermofluids* **2022**, *15*, 100189. [CrossRef]
12. Wang, D.; Fan, B.; Chen, Y.; Han, Y.; Liu, Y.; Wang, Y.; Liu, H.; Jiao, X. Comparative analysis of heat loss performance of flat plate solar collectors at different altitudes. *Sol. Energy* **2022**, *244*, 490–506. [CrossRef]
13. Al-Tabbakh, A.A. Numerical transient modeling of a flat plate solar collector. *Results Eng.* **2022**, *15*, 100580. [CrossRef]
14. Wang, D.; Mo, Z.; Liu, Y.; Ren, Y.; Fan, J. Thermal performance analysis of large-scale flat plate solar collectors and regional applicability in China. *Energy* **2022**, *238*, 121931. [CrossRef]

15. Thakur, A.; Kumar, S.; Kumar, P.; Kumar, S.; Bhardwaj, A.K. A review on the simulation/CFD based studies on the thermal augmentation of flat plate solar collectors. *Mater. Today Proc.* **2021**, *46*, 8578–8585. [CrossRef]

16. Vijay, R.; Vijayakumar, P.; Kumaresan, G.; Kumar, S.G. Performance study of FPSC integrated with twisted tape inserts. *Mater. Today Proc.* **2021**, *45*, 1222–1226. [CrossRef]

17. Zhang, D.; Tao, H.; Wang, M.; Sun, Z.; Jiang, C. Numerical simulation investigation on thermal performance of heat pipe flat-plate solar collector. *Appl. Therm. Eng.* **2017**, *118*, 113–126. [CrossRef]

18. Badiei, Z.; Eslami, M.; Jafarpur, K. Performance improvements in solar flat plate collectors by integrating with phase change materials and fins: A CFD modeling. *Energy* **2020**, *192*, 116719. [CrossRef]

19. Diez, F.J.; Navas-Gracia, L.M.; Martínez-Rodríguez, A.; Correa-Guimaraes, A.; Chico-Santamarta, L. Modelling of a flat-plate solar collector using artificial neural networks for different working fluid (water) flow rates. *Sol. Energy* **2019**, *188*, 1320–1331. [CrossRef]

20. Carmona, M.; Palacio, M. Thermal modelling of a flat plate solar collector with latent heat storage validated with experimental data in outdoor conditions. *Sol. Energy* **2019**, *177*, 620–633. [CrossRef]

21. Shafieian, A.; Khiadani, M.; Nosrati, A. Theoretical modelling approaches of heat pipe solar collectors in solar systems: A comprehensive review. *Sol. Energy* **2019**, *193*, 227–243. [CrossRef]

22. Azad, E. Theoretical and experimental investigation of heat pipe solar collector. *Exp. Therm. Fluid Sci.* **2008**, *32*, 1666–1672. [CrossRef]

23. Papoutsis, E.G.; Koronaki, I.P.; Papaefthimiou, V.D. Numerical simulation and parametric study of different types of solar cooling systems under Mediterranean climatic conditions. *Energy Build.* **2017**, *138*, 601–611. [CrossRef]

24. Naghavi, M.S.; Ong, K.S.; Badruddin, I.A.; Mehrali, M.; Silakhori, M.; Metselaar, H.S.C. Theoretical model of an evacuated tube heat pipe solar collector integrated with phase change material. *Energy* **2015**, *91*, 911–924. [CrossRef]

25. Ranjith, P.V.; Karim, A.A. A comparative study on the experimental and computational analysis of solar flat plate collector using an alternate working fluid. *Procedia Technol.* **2016**, *24*, 546–553. [CrossRef]

26. Nasrin, R.; Alim, M.A. Finite element simulation of forced convection in a flat plate solar collector: Influence of nanofluid with double nanoparticles. *J. Appl. Fluid Mech.* **2014**, *7*, 543–556.

27. Al-Rbaihat, R.; Sakhrieh, A.; Al-Asfar, J.; Alahmer, A.; Ayadi, O.; Al-Salaymeh, A.; Al-hamamre, Z.; Al-Bawwab, A.; Hamdan, M. Performance assessment and theoretical simulation of adsorption refrigeration system driven by flat plate solar collector. *JJMIE* **2017**, *11*, 1–11.

28. Müller, S.; Giovannetti, F.; Reineke-Koch, R.; Kastner, O.; Hafner, B. Simulation study on the efficiency of thermochromic absorber coatings for solar thermal flat-plate collectors. *Sol. Energy* **2019**, *188*, 865–874. [CrossRef]

29. Aggarwal, S.; Kumar, R.; Kumar, S.; Bhatnagar, M.; Kumar, P. Computational fluid dynamics-based analysis for optimization of various thermal enhancement techniques used in evacuated tubes solar collectors: A review. *Mater. Today Proc.* **2021**, *46*, 8700–8707. [CrossRef]

30. Jiandong, Z.; Hanzhong, T.; Susu, C. Numerical simulation for structural parameters of flat-plate solar collector. *Sol. Energy* **2015**, *117*, 192–202. [CrossRef]

31. Herez, A.; El Hage, H.; Lemenand, T.; Ramadan, M.; Khaled, M. Review on photovoltaic/thermal hybrid solar collectors: Classifications, applications and new systems. *Sol. Energy* **2020**, *207*, 1321–1347. [CrossRef]

32. del Amo, A.; Martínez-Gracia, A.; Bayod-Rújula, A.A.; Antoñanzas, J. An innovative urban energy system constituted by a photovoltaic/thermal hybrid solar installation: Design, simulation and monitoring. *Appl. Energy* **2017**, *186*, 140–151. [CrossRef]

33. Hazami, M.; Riahi, A.; Mehdaoui, F.; Nouicer, O.; Farhat, A. Energetic and energetic performance analysis of a PV/T (photovoltaic thermal) solar system tested and simulated under Tunisian (North Africa) climatic conditions. *Energy* **2016**, *107*, 78–94. [CrossRef]

34. Lämmle, M.; Kroyer, T.; Fortuin, S.; Wiese, M.; Hermann, M. Development and modeling of highly efficient PVT collectors with low-emissivity coatings. *Sol. Energy* **2016**, *130*, 161–173. [CrossRef]

35. Gallero, F.J.G.; Maestre, I.R.; Hemida, H.; Gómez, P.Á. Practical approaches to assess thermal performance of a finned heat sink prototype for low concentration photovoltaics (LCPV) systems: Analytical correlations vs. CFD modelling. *Appl. Therm. Eng.* **2019**, *156*, 220–229. [CrossRef]

36. Choi, H.U.; Choi, K.H. Numerical study on the performance of a solar-assisted heat pump coupled with a photovoltaic-thermal air heater. *Energy* **2023**, *285*, 129480. [CrossRef]

37. Vittorini, D.; Cipollone, R. Fin-cooled photovoltaic module modeling–Performances mapping and electric efficiency assessment under real operating conditions. *Energy* **2019**, *167*, 159–167. [CrossRef]

38. Charalambous, P.G.; Maidment, G.G.; Kalogirou, S.A.; Yiakoumetti, K. Photovoltaic thermal (PV/T) collectors: A review. *Appl. Therm. Eng.* **2007**, *27*, 275–286. [CrossRef]

39. Wu, J.; Zhang, X.; Shen, J.; Wu, Y.; Connelly, K.; Yang, T.; Wang, H. A review of thermal absorbers and their integration methods for the combined solar photovoltaic/thermal (PV/T) modules. *Renew. Sustain. Energy Rev.* **2017**, *75*, 839–854. [CrossRef]

40. Srithar, K.; Akash, K.; Nambi, R.; Vivar, M.; Saravanan, R. Enhancing photovoltaic efficiency through evaporative cooling and a solar still. *Sol. Energy* **2023**, *265*, 112134. [CrossRef]

41. Elbreki, A.M.; Sopian, K.; Fazlizan, A.; Ibrahim, A. An innovative technique of passive cooling PV module using lapping fins and planner reflector. *Case Stud. Therm. Eng.* **2020**, *19*, 100607. [CrossRef]

42. Calise, F.; d'Accadia, M.D.; Vanoli, L. Design and dynamic simulation of a novel solar trigeneration system based on hybrid photovoltaic/thermal collectors (PVT). *Energy Convers. Manag.* **2012**, *60*, 214–225. [CrossRef]

43. Haiping, C.; Haowen, L.; Heng, Z.; Kai, L.; Xinxin, G.; Boran, Y. Numerical simulation and experimental analysis of an LCPV/T system under real operating conditions. *J. Clean. Prod.* **2019**, *209*, 903–915. [CrossRef]

44. Yang, L.; Heng, Z.; Haiping, C.; Han, Y.; Fei, Y. Simulating and experimental research on a low-concentrating PV/T triple-generation system. *Energy Convers. Manag.* **2019**, *199*, 111942. [CrossRef]

45. Da Silva, R.M.; Fernandes, J.L.M. Hybrid photovoltaic/thermal (PV/T) solar systems simulation with Simulink/Matlab. *Sol. Energy* **2010**, *84*, 1985–1996. [CrossRef]

46. Abdullah, A.L.; Misha, S.; Tamaldin, N.; Rosli, M.A.M.; Sachit, F.A. Hybrid photovoltaic thermal PVT solar systems simulation via Simulink/Matlab. *CFD Lett.* **2019**, *11*, 64–78.

47. Brekke, N.; Otanicar, T.; DeJarnette, D.; Hari, P. A parametric investigation of a concentrating photovoltaic/thermal system with spectral filtering utilizing a two-dimensional heat transfer model. *J. Sol. Energy Eng.* **2016**, *138*, 021007. [CrossRef]

48. Karathanassis, I.K.; Papanicolaou, E.; Belessiotis, V.; Bergeles, G.C. Dynamic simulation and exergetic optimization of a Concentrating Photovoltaic/Thermal (CPVT) system. *Renew. Energy* **2019**, *135*, 1035–1047. [CrossRef]

49. Alves, P.; Fernandes, J.F.; Torres, J.P.N.; Branco, P.C.; Fernandes, C.; Gomes, J. From Sweden to Portugal: The effect of very distinct climate zones on energy efficiency of a concentrating photovoltaic/thermal system (CPV/T). *Sol. Energy* **2019**, *188*, 96–110. [CrossRef]

50. Widyolar, B.K.; Abdelhamid, M.; Jiang, L.; Winston, R.; Yablonovitch, E.; Scranton, G.; Cygan, D.; Abbasi, H.; Kozlov, A. Design, simulation and experimental characterization of a novel parabolic trough hybrid solar photovoltaic/thermal (PV/T) collector. *Renew. Energy* **2017**, *101*, 1379–1389. [CrossRef]

51. Moh'd A, A.N. Modeling of a novel concentrated PV/T distillation system enhanced with a porous evaporator and an internal condenser. *Sol. Energy* **2015**, *120*, 593–602.

52. Korres, D.N.; Papingiotis, T.; Koronaki, I.; Tzivanidis, C. Thermal and Optical Analyses of a Hybrid Solar Photovoltaic/Thermal (PV/T) Collector with Asymmetric Reflector: Numerical Modeling and Validation with Experimental Results. *Sustainability* **2023**, *15*, 9932. [CrossRef]

53. Liu, L.; Jia, Y.; Lin, Y.; Alva, G.; Fang, G. Numerical study of a novel miniature compound parabolic concentrating photovoltaic/thermal collector with microencapsulated phase change slurry. *Energy Convers. Manag.* **2017**, *153*, 106–114. [CrossRef]

54. Tripathi, R.; Tiwari, G.N.; Al-Helal, I.M. Thermal modelling of N partially covered photovoltaic thermal (PVT)–Compound parabolic concentrator (CPC) collectors connected in series. *Sol. Energy* **2016**, *123*, 174–184. [CrossRef]

55. Dehghan, M.; Vajedi, H.; Rahgozar, S.; Karimi, N. Energy, economic, and environmental analysis of converging air-based photovoltaic-thermal (air/PV-T) systems: A yearly benchmarking. *J. Clean. Prod.* **2024**, *434*, 139871. [CrossRef]

56. Sheikholeslami, M.; Ghasemian, M.; Dehghan, M. Numerical simulation and Enviro-economic examination of Photovoltaic system in presence of complex shape of tube equipped with turbulator. *Renew. Energy* **2024**, *231*, 120977. [CrossRef]

57. Khelifa, A.; Attia, M.E.H.; Driss, Z.; Manokar, A.M. Performance enhancement of photovoltaic solar collector using fins and bi-fluid: Thermal efficiency study. *Sol. Energy* **2023**, *263*, 111987. [CrossRef]

58. Aydın, A.; Kayri, İ.; Aydin, H. Electrical and thermal performance enhancement of a photovoltaic thermal hybrid system with a novel inner plate-finned collective cooling with different nanofluids. *Int. J. Green Energy* **2024**, *21*, 555–569. [CrossRef]

59. Manrique, J.A. Energía solar. In *Fundamentos y Aplicaciones Fototérmicas*; No. 621.47 M3; Ed. Harla: Mexico City, Mexico, 1984.

60. Gasquet, H.L. *Conversión de la Luz Solar en Energía Eléctrica–Manual Teórico Practico*; Chapter 4; Gasquet: Mexico City, Mexico, 2004; pp. 17–32.

61. Singh, P.; Ravindra, N.M. Analysis of series and shunt resistance in silicon solar cells using single and double exponential models. *Emerg. Mater. Res.* **2012**, *1*, 33–38. [CrossRef]

62. Sukamongkol, Y.; Chungpaibulpatana, S.; Limmeechokchai, B.; Sripadungtham, P. A simulation model for predicting the transient performance of a hybrid pv/t forced-circulation solar water-heating system. In Proceedings of the 8th World Renewable Energy Congress, Denver, CO, USA, 28 August–3 September 2004.

63. Michael, J.J.; Iniyan, S.; Goic, R. Flat plate solar photovoltaic–thermal (PV/T) systems: A reference guide. *Renew. Sustain. Energy Rev.* **2015**, *51*, 62–88. [CrossRef]

64. ANSYS. *ANSYS Fluent Theory Guide*; ANSYS Inc.: Canonsburg, PA, USA, 2019.

65. Perez Grajales, S.G.; Hernández, A.H.; Juárez-Romero, D.; Lopez Lopez, G.; Urquiza-Beltran, G. Design, Construction, and Characterization of a Solar Photovoltaic Hybrid Heat Exchanger Prototype. *Processes* **2024**, *12*, 588. [CrossRef]